THE JOURNAL OF PHYSICAL CHEMISTRY B

Article

pubs.acs.org/JPCB

Synthesis and Controlled Self-Assembly of UV-Responsive Gold Nanoparticles in Block Copolymer Templates

Dong-Po Song, Xinyu Wang, Ying Lin, and James J. Watkins*

Department of Polymer Science and Engineering, University of Massachusetts Amherst, 120 Governors Drive, Amherst, Massachusetts 01003, United States

Supporting Information

ABSTRACT: We demonstrate the facile synthesis of gold nanoparticles (GNPs) functionalized by UV-responsive block copolymer ligands, poly(styrene)-*b*-poly(*o*-nitrobenzene acrylate)-SH (PS-*b*-PNBA-SH), followed by their targeted distribution within a lamellae-forming poly(styrene)-*b*-poly(2-vinylpyridine) (PS-*b*-P2VP) block copolymer. The multilayer, micelle-like structure of the GNPs consists of a gold core, an inner PNBA layer, and an outer PS layer. The UV-sensitive PNBA segment can be deprotected into a layer containing poly(acrylic acid) (PAA) when exposed to UV light at 365 nm, which enables the simple and precise tuning of GNP surface properties from hydrophobic to amphiphilic. The GNPs bearing ligands of different chemical compositions were successfully and selectively incorporated into the PS-*b*-P2VP block copolymer, and UV light showed a profound influence on the spatial distributions of GNPs. Prior to UV exposure, GNPs partition along the interfaces of PS and P2VP domains, while the UV-treated GNPs are incorporated into P2VP domains as a result of hydrogen bond interactions between PAA on the gold surface and P2VP domains. This provides an easy way of controlling the arrangement of nanoparticles in polymer matrices by tailoring the nanoparticle surface using UV light.

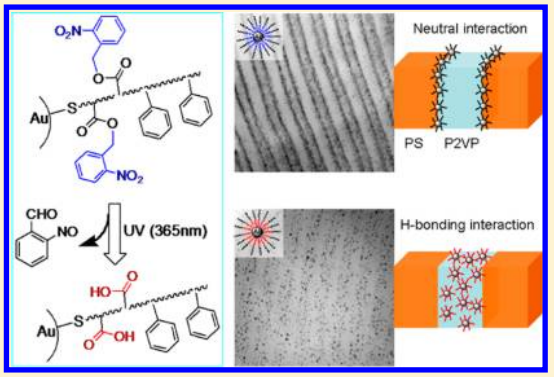

INTRODUCTION

The hierarchical assembly of inorganic nanoparticles within microphase-separated block copolymer (BCP) matrices has been intensively studied to create novel functional hybrid materials, such as high-performance catalysts, photonic crystals, chemical sensors, and electronic devices, and for other applications.[1−8] However, the precise control over the arrangement of nanoparticles in polymer matrices remains challenging yet critical to the properties of the resulting hybrid materials. The distribution of nanoparticles in a BCP greatly depends on a delicate balance of the enthalpic contributions arising from the interactions between nanoparticle ligands and BCP segments, and the entropic contributions including penalties due to polymer chain stretching to accommodate the nanoparticles.[5,9−14] Chemical modification of nanoparticle surface properties has proven to be an effective approach to sequestering nanoparticles in selected domains of block copolymer templates by introducing favorable interactions between the surface ligands and specific blocks. Kramer and coworkers demonstrated a precise control of gold nanoparticle location in poly(styrene-*block*-2-vinylpyridine) (PS-*b*-P2VP) copolymers by using a mixture of low molecular weight thiol end-functional PS and P2VP oligomers as the surface ligand.[10,15−21] Varying the PS and P2VP surface compositions allows placement of the nanoparticles into PS or P2VP microdomains or at the interface. The localization is mainly based on optimizing the enthalpic interaction of nanoparticles with the BCP segments by tailoring the nanoparticle surface with components compatible with the specific blocks.[10,17] Nanoparticle size has been found to show a strong influence on nanoparticle location in BCP templates for entropic reasons. Thomas et al. have shown that large silica nanoparticles segregated to the center of one domain, whereas smaller gold nanoparticles (GNPs) segregated at the interface between microdomains, suggesting that the self-assembly process was strongly influenced by entropic contributions.[9]

Hydrogen bonding is an interesting tool for the assembly of BCP based hybrid materials due to its specific, directional, and reversible characteristics.[22−28] The compatibility between host polymers and guest additives can be greatly enhanced by the formation of multiple hydrogen bonds (H-bonds) to avoid macrophase separation. In particular, H-bonding has been employed for the coassembly of nanoparticles and BCPs. For example, Russell, Emrick, et al. conducted a systematic study on hybrid thin films of PS-*b*-P2VP and nanoparticles, and by variation of surface ligands and processing methods, nanoparticles possessing both hydrophobic and hydrophilic ligands (hydroxyl groups) can be dispersed either within one of the microdomains or at the interface.[29] Recently, Xu and coworkers reported an approach to achieve the well ordered

Received: August 13, 2014
Revised: October 10, 2014
Published: October 16, 2014

dx.doi.org/10.1021/jp508212f | J. Phys. Chem. B 2014, 118, 12788−12795

Scheme 1. Synthesis of UV-Responsive GNPs Coated with Polystyrene-*b*-poly(*o*-nitrobenzyl acrylate)-SH (PS-*b*-PNBA-SH) Block Copolymer Ligands

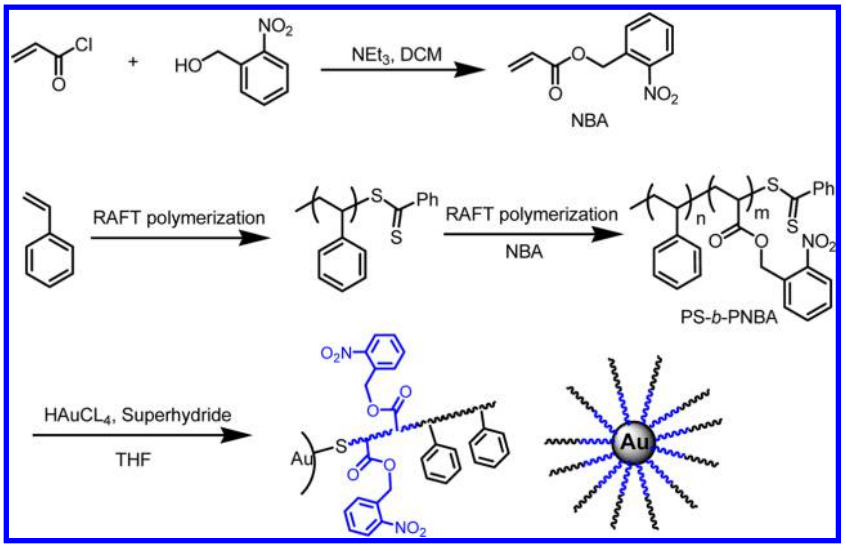

BCP/nanoparticle hybrid materials by using small molecules that have the H-bonding capability with BCP segments while exhibiting neutral interactions with nanoparticles.[30] Our group demonstrated a H-bonding strategy to incorporate gold or silicon nanoparticles at high loadings into poly(styrene-*block*-ethylene oxide) (PS-*b*-PEO) or poly(ethylene oxide-*b*-propylene oxide-*b*-ethylene oxide) (PEO-*b*-PPO-*b*-PEO).[31−33] Additives with strong interactions with one of the blocks have been shown to significantly increase segregation strength resulting in highly filled, well ordered composites.[34−37] In addition to the small molecule H-bonding ligands, H-bond-donating polymers have also been reported to serve as the ligands for nanoparticles. Hawker et al. have succeeded in the design and synthesis of GNPs capped with random copolymers or BCPs that have hydroxyl functionalities on polymer chains.[38,39] GNPs were coated with thiol-terminated poly(styrene-*b*-1,2/3,4-isoprene) diblock copolymer ligands which were then hydroxylated by hydroboration reaction.[38] These nanoparticles have an inner shell with hydroxyl groups (PIOH) enabling the control of nanoparticle segregation in PS-*b*-P2VP matrix by H-bonding, and an outer layer of PS providing a good solubility of nanoparticles in nonpolar organic solvents which can greatly benefit the processability of nanoparticle/BCP mixture.

In this work, we develop photoresponsive GNPs to achieve precise control over their arrangement in polymer matrices using UV light. We demonstrate the simple synthesis of micelle-like GNPs capped with UV-sensitive BCPs poly(styrene)-*b*-poly(*o*-nitrobenzene acrylate) (PS-*b*-PNBA−S-Au). The inner layer (PNBA) can be deprotected into a highly hydrophilic block containing poly(acrylic acid) (PAA) when exposed to UV light at 365 nm. A lamellae-forming PS-*b*-P2VP BCP was used as the template for the assembly of these GNPs. Before UV irradiation, the NPs partition along the interface of PS and P2VP domains, while the GNPs after UV exposure are incorporated into the P2VP domain due to strong H-bonding interactions between PAA on gold surface and P2VP of the PS-*b*-P2VP matrix.

EXPERIMENTAL SECTION

Materials. Acryloyl chloride (97%), 2-nitrobenzyl alcohol (97%), triethylamine (>99%), 2-cyano-2-propyl benzodithioate (>97%), hydrogen tetrachloroaurate(III) hydrate (>99%), and Super-Hydride solution (1.0 M lithium triethylborohydride in THF) were purchased from Sigma-Aldrich and used without further purification. Azobis(isobutyronitrile) (AIBN, Aldrich) was recrystallized from methanol. Styrene (Sigma-Aldrich, >99%) was purified by passage through a basic aluminum oxide column prior to use. Anhydrous tetrahydrofuran (>99%, H_2O < 50 ppm) and anhydrous dichloromethane (>99%, H_2O < 50 ppm) were bought from Acros Organics. Lamellae-forming (199 kg/mol with $f_{P2VP} \sim 0.48$) PS-*b*-P2VP block copolymer was purchased from Polymer Source.

Synthesis of *o*-Nitrobenzyl Acrylate (NBA). Into a dry flask were added *o*-nitrobenzyl alcohol (8.42 g, 55 mmol) and Et_3N (7.8 mL, 56 mmol) followed by anhydrous CH_2Cl_2 (50 mL). Under N_2 atmosphere, the resulting mixture was kept in an ice bath for about 30 min before addition of acryloyl chloride (4.4 mL, 55 mmol) (Scheme 1). The mixture was allowed to warm up to rt and was stirred for 24 h. The mixture was washed with water, the organic phase was dried over $MgSO_4$ and filtered, and then the solvent was removed in vacuum. The yellow−brown crude product was purified by chromatography on silica gel, affording a viscous colorless liquid (10.2 g, yield: 90%). ^{1}H NMR (300 MHz, CDCl3): δ 8.12 (d, 1H, J = 8.4 Hz, Ar−H), 7.63 (m, 2H, Ar−H), 7.50 (t, 1H, J = 7.8 Hz, Ar−H), 6.50 (dd, 1H, J = 17.3 Hz,1.2 Hz, ═CH_2, trans), 6.30 (dd, 1H, J = 17.3 Hz, 10.4 Hz, ═CH), 5.93 (dd, 1H, J = 10.4 Hz, 1.2 Hz, ═CH_2, cis), 5.62 (s, 2H, O−CH_2−).

Synthesis of PS-RAFT by RAFT Polymerization. Into an oven-dried flask were added styrene (15 mL, 131 mmol) and 2-cyano-2-propyl benzodithioate (0.14 mL, 0.72 mmol) forming a red solution. The deoxygenation of the solution was achieved by nitrogen purging for at least 30 min. The polymerization was initiated by heating the solution to 110 °C, and the solution was stirred for different time periods to obtain different molecular weights (MWs) of PS. At the end of polymerization, the mixture was cooled to rt followed by adding THF to quench the reaction. PS-RAFT products were obtained by pouring the THF solution into methanol.

Synthesis of PS-*b*-PNBA-RAFT by RAFT Polymerization. PS-RAFT (0.5 mmol), NBA (3.3 g, 15 mmol) and

dx.doi.org/10.1021/jp508212f | J. Phys. Chem. B 2014, 118, 12788−12795

AIBN (17.6 mg, 0.1 mmol) were added into a dry flask followed by 4 mL of toluene. The resulting mixture was purged by nitrogen flow for at least 30 min to get rid of oxygen and then was kept at 80 °C to initiate the polymerization. The control of total molecular weight of the resulting block copolymer was realized simply by variation of reaction time. In the end, THF was added into the solution to quench the polymerization, and the copolymer was then precipitated in methanol and dried under vacuum. The molecular weight (M_n) and polydispersity index (PDI) of the block copolymer PS-*b*-PNBA-RAFT were measured by gel permeation chromatography (GPC, calibrated by PS standards) using THF as the eluent. The compositions of the copolymers were calculated from ^{1}H NMR based on the peak area of PS (broad peaks from 6.4 to 7.1 ppm) compared to that of CH_2 bonded to the 2-nitrobenzyl group (broad peak centered at 5.3 ppm). The number of PS repeating units was calculated by the expression (M_n of PS)/104, while the NBA number was calculated from the number of PS repeating units and the molar ratio of NBA to styrene units.

Synthesis of GNPs Coated with PS-*b*-PNBA-SH. PS-*b*-PNBA-RAFT copolymers were used directly in the preparation of Au nanoparticles using the THF one-phase method.[40] Au precursor ($HAuCl_4 \cdot 3H_2O$, 0.4 mmol) and 0.2 mmol of PS-*b*-PNBA-RAFT copolymers were placed in a flame-dried Schlenk flask with a magnetic stirrer. Anhydrous THF (40 mL) was injected into the flask, forming a yellow solution via a syringe under agitation after three vacuum and nitrogen purging cycles. GNPs were synthesized by adding 4.8 mmol of the reducing agent, Super-Hydride ($Li(C_2H_5)_3BH$ in THF), dropwise in 20 min under dry nitrogen. The solution immediately turned dark brown upon adding the reducing agent, and the resulting solution was stirred for an additional 3 h to achieve a complete reaction. The free polymer ligands were separated from the polymer brush coated Au nanoparticles by centrifugation using a mixture of THF and methanol followed by precipitation in hexane. The washed Au nanoparticles were collected as dark red powder.

Preparation of PS-*b*-P2VP/Au Nanoparticles Composites. A lamellae-forming PS-*b*-P2VP (199 kg/mol, $f_{P2VP} \sim 0.48$) block copolymer was used as the template for the assembly of GNPs. Into a freshly prepared PS-*b*-P2VP diblock copolymer solution (1 wt % in chloroform) were added GNPs forming a mixture with a certain weight ratio. Films of the block copolymer or block copolymer/nanoparticle composites were prepared by drop casting the solutions onto glass slides. The resulting films were annealed in saturated dichloromethane (DCM) vapor at room temperature for at least 3 days.

UV deprotection was carried out by the exposure of dried GNP films to UV light of 365 nm (about 3 mW/cm^2) for at least 65 h. The GNP films were prepared by drop-casting and evaporation of THF solutions on glass slides. The nanoparticle powders after UV radiation were mixed with PS-*b*-P2VP block copolymer in $CHCl_3$, and the composite films were obtained by drop-casting and evaporation of the solution on glass slides. The obtained films were annealed in saturated DCM vapor at room temperature for at least 3 days.

Transmission Electron Microscopy (TEM). After annealing, the films of PS-*b*-P2VP/GNPs composites were removed from the glass slides and embedded into epoxy resin. Thin sections of approximately 50 nm in thickness for TEM were prepared using a Leica Ultracut UCT microtome operated at room temperature. Bright field TEM measurements were conducted with a JEOL 2000FX TEM operated at accelerating voltages of 200 kV.

Other Characterizations. Proton nuclear magnetic resonance (^{1}H NMR) spectra were recorded on a Bruker-Spectrospin at 300 MHz. Infrared spectroscopic measurements were recorded with a Bruker Vertex 70 FTIR spectrophotometer. Gel permeation chromatography (GPC) measurements of block copolymers were carried out using a Polymer Labotatories PL-GPC50 instrument with two 5 μm mixed-D columns, a 5 μm guard column, and a RI detector (HP1047A). THF was used as the eluent at a flow rate of 1.0 mL/min. Polystyrene standards were used for the calibration. Thermogravimetric Analysis (TGA) experiments were performed on a TGA2950 thermogravimetric analyzer with a heating rate of 10 °C/min under N_2 atmosphere.

RESULTS AND DISCUSSION

Polymers and polymer composites featuring photolabile groups are under intense research because they allow the alteration of polymer properties and morphology simply by irradiation. Phase segregation and phase mixing in block copolymers upon irradiation, for example, can be induced by simple deprotection of additives or one of the blocks.[41−43] Among the many photolabile groups that have been studied, *o*-nitrobenzyl (*o*-NB) group is a popular choice in the areas of synthetic organic chemistry and materials science.[43] The *o*-NB groups are usually used to impart a stimulus responsive character to the polymer, allowing a switching in polarity from the hydrophobic "protected" form to the hydrophilic "deprotected" form. The photodeprotection of *o*-NB esters usually yields an *o*-nitrosobenzaldehyde, simultaneously releasing a free carboxylic acid as the hydrogen donator for H-bonds.[44,45] As shown in Scheme 1, *o*-nitrobenzyl acrylate (NBA) has been chosen as the photolabile monomer for the synthesis of photoresponsive BCP ligand. Although NBA was considered to be a challenge for controlled radical polymerization (CRP),[46] we have been successful in the preparation of PS-*b*-PNBA BCPs in a controlled manner using the RAFT method. As shown in Figure 1, GPC IR traces show unimodal molecular weight

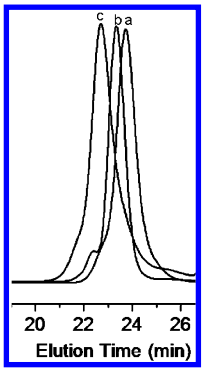

Figure 1. GPC RI traces of polystyrene-*b*-poly(*o*-nitrobenzyl acrylate)-RAFT block copolymers: (a) PS_{23}-*b*-$PNBA_9$-S(CS)Ph; (b) PS_{40}-*b*-$PNBA_5$-S(CS)Ph; (c) PS_{23}-*b*-$PNBA_{15}$-S(CS)Ph.

distributions of the obtained BCPs, and the PDIs are less than 1.2, indicating a good control over the polymerization of NBA. The molecular weight information on these BCPs has been summarized in Table 1. Average numbers of styrene repeating units per chain were calculated according to the expression (M_n of PS)/104, while the number of NBA repeating units was

dx.doi.org/10.1021/jp508212f | J. Phys. Chem. B 2014, 118, 12788−12795

Table 1. Characterization of Polystyrene-*b*-poly(*o*-nitrobenzyl acrylate) (PS-*b*-PNBA) Block Copolymer Ligands

	PS (GPC)[a]		PS-*b*-PNBA-S(CS)Ph (GPC)[a]			
	M_n (kg/mol)	PDI	M_n (kg/mol)	PDI	N_S[b]	N_{NBA}[b]
PS_{23}-*b*-$PNBA_{15}$-S(CS)Ph	2.4	1.08	4.9	1.16	23	15
PS_{23}-*b*-$PNBA_9$-S(CS)Ph	2.4	1.08	3.7	1.11	23	9
PS_{40}-*b*-$PNBA_5$-S(CS)Ph	4.2	1.06	4.7	1.07	40	5

[a]Determined by GPC vs polystyrene standards. [b]Average numbers of styrene and *o*-nitrobenzyl acrylate repeating units per chain calculated by GPC and ^{1}H NMR, respectively.

obtained from the number of PS repeating units and the molar ratio of NBA to styrene units based on ^{1}H NMR spectrum.

As shown in Scheme 1, the obtained copolymers (PS-*b*-PNBA-S(CS)Ph) were directly used as the ligand for the synthesis of GNPs. Super-Hydride ($Li(C_2H_5)_3BH$ in THF) was chosen as the reducing agent for both gold precursor ($HAuCl_4$) and RAFT ends of polymer ligand. Upon addition of Super-Hydride, the color of the gold precursor/polymer ligand mixture turned immediately from yellow into brown, indicating the formation of GNPs. It is important to note that the addition of Super-Hydride should be careful and slow to prevent PNBA block from reduction. The survival of *o*-NB ester units was confirmed by ^{1}H NMR as well as FTIR spectra of the obtained GNPs. The multi peaks at 7.4−8.0 ppm in Figure 2 ascribed to

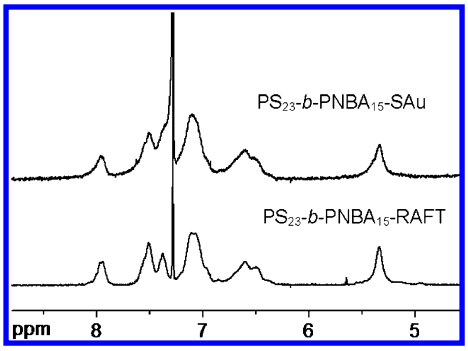

Figure 2. ^{1}H NMR spectra of a BCP ligand (PS_{23}-*b*-$PNBA_{15}$-RAFT) and GNPs (PS_{23}-*b*-$PNBA_{15}$-SAu).

aromatic hydrogen (Ar−H) of *o*-NB group together with the *o*-$NBCH_2$ broad peak centered at 5.3 ppm are observed in the ^{1}H NMR spectra of GNPs (PS_{23}-*b*-$PNBA_{15}$-SAu). Figure 3 shows the FTIR spectrum of GNPs (PS_{23}-*b*-$PNBA_9$-SAu) before UV irradiation indicating the presence of C═O (1737 cm^{-1}) on the gold surface. In comparison with the reported procedure of GNP synthesis,[39] one improvement of the method here is the avoidance of highly toxic hydrazine, which was typically used to reduce the RAFT ends into thiol groups before GNP synthesis.

PS-*b*-PNBA-RAFT BCPs with various molecular weights and chemical compositions were used in the gold nanoparticle synthesis. As shown in Table 1, average numbers of styrene (N_s) and NBA (N_{NBA}) repeating units per chain were calculated according to GPC and ^{1}H NMR data (see Table 1). By varying the N_s and N_{NBA}, we can build the inner layer PNBA and the outer layer PS on the gold surface with tunable thicknesses.

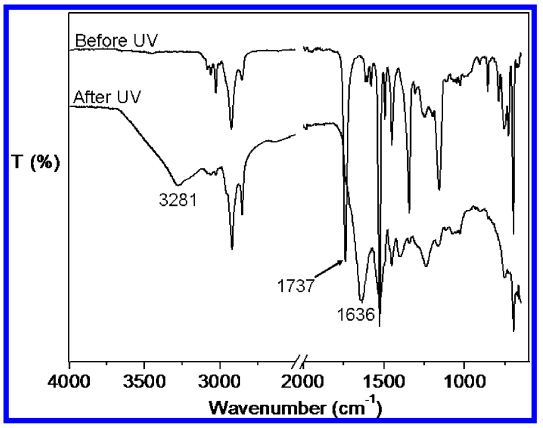

Figure 3. FTIR spectra of GNPs (PS_{23}-*b*-$PNBA_9$-SAu) before and after UV irradiation.

PS_{23}-*b*-$PNBA_{15}$-RAFT was chosen to investigate the influence of ligand/Au molar ratio on the average nanoparticle core diameters (D_{core}). The D_{core} was obtained from image analysis based on TEM images for at least 200 GNPs, and a decrease from 3.8 ± 1.7 nm to 3.1 ± 1.0 nm was observed with the variation of ligand/Au molar ratio from 1/4 to 1/3 (see TEM images and core size distributions in Figure S1, Supporting Information). Further increase of the ligand/Au molar ratio to 1/2 results in well-controlled core sizes around 2.5 nm with narrow size distributions (see Figure 4). Variation of molecular

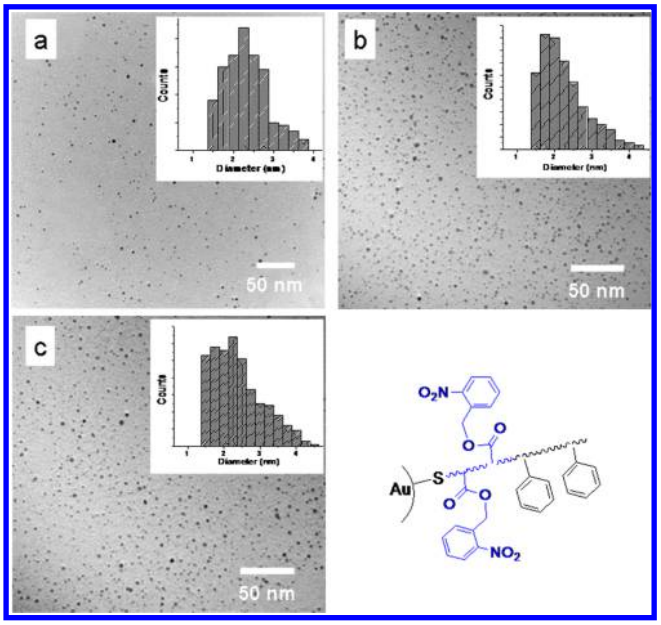

Figure 4. TEM images and corresponding core size distributions of GNPs bearing PS-*b*-PNBA ligands of different chemical compositions (a, PS_{23}-*b*-$PNBA_{15}$S-Au, D_{core} = 2.5 ± 0.6 nm; b, PS_{23}-*b*-$PNBA_9$S-Au, D_{core} = 2.4 ± 0.7 nm; c, PS_{40}-*b*-$PNBA_5$S-Au, D_{core} = 2.5 ± 0.7 nm).

weight and chemical composition of copolymer ligand shows limited influence on core size as well as distribution. According to the analyses of TEM images in Figure 4, average core sizes at 2.4 ± 0.7 and 2.5 ± 0.7 nm have been achieved by using PS_{23}-*b*-$PNBA_9$-RAFT and PS_{40}-*b*-$PNBA_5$-RAFT as the ligands. D_{core} was used to calculate the average surface area per gold nanoparticle. Weight fractions of gold and polymer ligands were measured by TGA and converted into volume fractions

dx.doi.org/10.1021/jp508212f | J. Phys. Chem. B 2014, 118, 12788−12795

based on the density of the polymer (~1.05 g/cm^3) and the density of the gold (~19.3 g/cm^3). The number of polymer ligands per gold particle divided by the average surface area of the gold particles gives the areal chain density of polymer ligands on the particle surface.[47] The values are 2.2, 2.5, and 1.3 chains/nm^2 for GNPs PS_{23}-*b*-$PNBA_{15}$S-Au, PS_{23}-*b*-$PNBA_9$S-Au and PS_{40}-*b*-$PNBA_5$S-Au, respectively. The obtained GNPs after purification can be redispersed in many nonpolar organic solvents such as chloroform, dichloromethane (DCM), and THF benefiting from the PS outer layer of the micelle-like structure.

The segregation behaviors of GNPs coated with PS-*b*-PNBA BCPs were investigated by using a lamellae-forming PS-*b*-P2VP BCP matrix (199 kg/mol, $f_{p2vp} \sim 0.48$). For the BCP-GNP composites, we typically prepared a 1 wt % polymer solution in chloroform admixed with GNPs with expected weight fractions in the solid. Herein the weight percentage (wt %) of GNPs in the composites is based on the mass of the NP core and ligand shell. Briefly, the composite films on glass slides were obtained by drop-casting and evaporation of the mixture solutions on a horizontal stage. The dried films were annealed in saturated DCM vapor for at least 3 days. The distributions of GNPs in the microphase separated matrix were determined by TEM characterization of the thin films prepared by microtoming of epoxy-supported bulk samples (see Experimental Section for more details). As shown in Figure 5a, a well-ordered lamellar

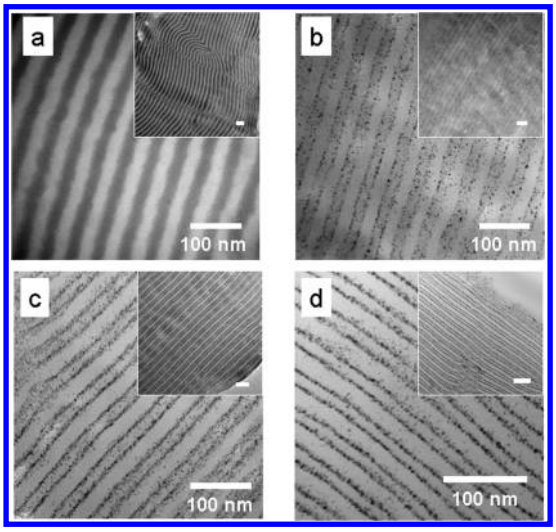

Figure 5. (a) TEM image of lamellae-forming PS-*b*-P2VP block copolymer (199 kg/mol, $f_{p2vp} \sim 0.48$) with I_2-stained P2VP appearing as the darker areas. TEM images of the composites containing GNPs capped with PS-*b*-PNBA ligands of different chemical compositions: (b) PS_{23}-*b*-$PNBA_{15}$S-Au; (c) PS_{23}-*b*-$PNBA_9$S-Au; (d) PS_{40}-*b*-$PNBA_5$S-Au. The weight percentage of GNPs in these composites is 15 wt %. Scale bars in the insets are 100 nm.

morphology was formed by the PS-*b*-P2VP BCP with the lighter areas being PS domains and the darker gray regions corresponding to iodine-stained P2VP domains. Figure 5b–d illustrates the locations of GNPs with different ligands in the same PS-*b*-P2VP BCP including (b) PS_{23}-*b*-$PNBA_{15}$S-Au, (c) PS_{23}-*b*-$PNBA_9$S-Au, and (d) PS_{40}-*b*-$PNBA_5$S-Au. Generally these GNPs show the same tendency to segregate along the PS/P2VP interfaces. It is reported that the distribution of GNPs with PS ligands is highly dependent on areal chain densities of ligands (Σ).[16,21,47,48] The interfacial absorption of GNPs will occur when the Σ is lower than a critical value (Σ_C).[16] In our case, the segregation along the interface of PS/P2VP (Figure 5b,c) was still observed for the nanoparticles with high Σs 2.2 and 2.5 chains/nm^2. The probable interaction between the inner PNBA layer of GNPs and the P2VP block of PS-*b*-P2VP is a likely reason for the interfacial absorption. This is similar to the results reported by Jang et al. that micelle-like GNPs with high Σ were sequestered at the PS/P2VP interface due to the much lower effective areal chain densities of ligands (Σ_{eff}) on the surface of inner shell.[38] For GNPs in the sample of Figure 5d, we aimed to build a thicker PS outer layer (N_{PS} = 40) and a thinner PNBA inner layer (N_{PNBA} = 5) on the gold surface to avoid the interaction between PNBA and P2VP. However, a GNP with a much lower Σ (1.3 chains/nm^2) was obtained, and the favorable interaction between P2VP and the gold surface is mainly responsible for the formation of single nanoparticle layers along the PS/P2VP interfaces as indicated in Figure 5d. In addition, the segregation of small nanoparticles at the interface of a BCP with a large domain spacing is consistent with the reported theoretical simulations and experimental results.[9,49,50]

As shown in Scheme 2, the inner layer PNBA of these micelle-like GNPs can be deprotected into a highly hydrophilic

Scheme 2. Illustration of UV Deprotection of GNPs from Hydrophobic into Amphiphilic Properties as Well as the H-Bonding Interaction between the Ligand on Gold Surface and Pyridine Units of PS-*b*-P2VP Block Copolymer after the Deprotection

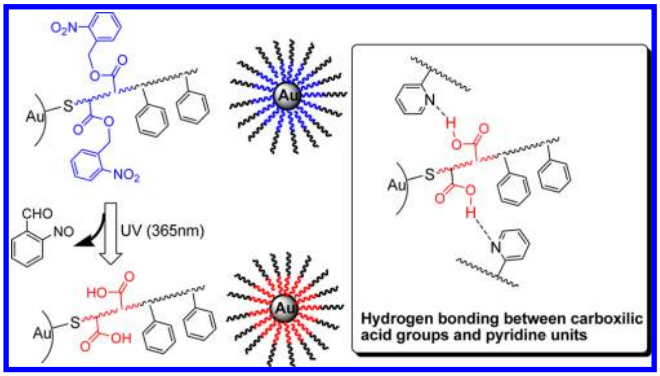

block containing poly(acrylic acid) (PAA) by simple exposure to UV light at 365 nm,[43−45] which provides an easy way of controlling nanoparticle locations by introducing H-bonding interactions between the acrylic acid functionalities of the GNP ligands and P2VP blocks of the PS-*b*-P2VP matrix. In order to investigate the effects of UV irradiation, it is necessary to minimize other favorable interactions between the GNPs and P2VP of the BCP matrix. In comparison with the other two samples of GNPs we prepared (PS_{40}-*b*-$PNBA_5$-SAu and PS_{23}-*b*-$PNBA_{15}$-SAu), GNP (PS_{23}-*b*-$PNBA_9$-SAu) is the best choice because it has a high areal chain density (2.5 chains/nm^2) of ligands to minimize the interaction between the pyridine units of the P2VP and the gold surface and a moderate PNBA content to create sufficient H-bond-donating functionalities after UV irradiation. The UV irradiation was carried out on dried GNP films prepared by casting and evaporation of their solutions on glass substrates (see Experimental Section for more details). Figure 3 shows the significant differences in the FTIR spectra of the GNPs before and after UV irradiation: the sharp and unimodal signal at 1737 cm^{-1} is assigned to the

dx.doi.org/10.1021/jp508212f | J. Phys. Chem. B 2014, 118, 12788−12795

carbonyl group (C═O) of PNBA before UV, while a red shift to 1636 cm^{-1} together with the appearance of a broad peak at 3281 cm^{-1} indicates the successful deprotection of PNBA into PAA by UV.

The GNPs (PS_{23}-*b*-$PNBA_9$-SAu) after UV irradiation can be redispersed in nonpolar organic solvent benefiting from the PS outer layer. This allows the preparation of a blend of the PS-*b*-P2VP BCP with the GNPs in chloroform to maximize H-bond interactions between PAA and P2VP. The obtained sample containing 20 wt % of GNPs was annealed in saturated DCM vapor for at least 3 days. Meanwhile, a blend of the PS-*b*-P2VP with the same amount of GNPs without UV exposure was made and annealed under the same conditions. TEM was used to investigate nanoparticle arrangement in PS-*b*-P2VP. As shown in Figure 6a, GNPs without UV irradiation mainly

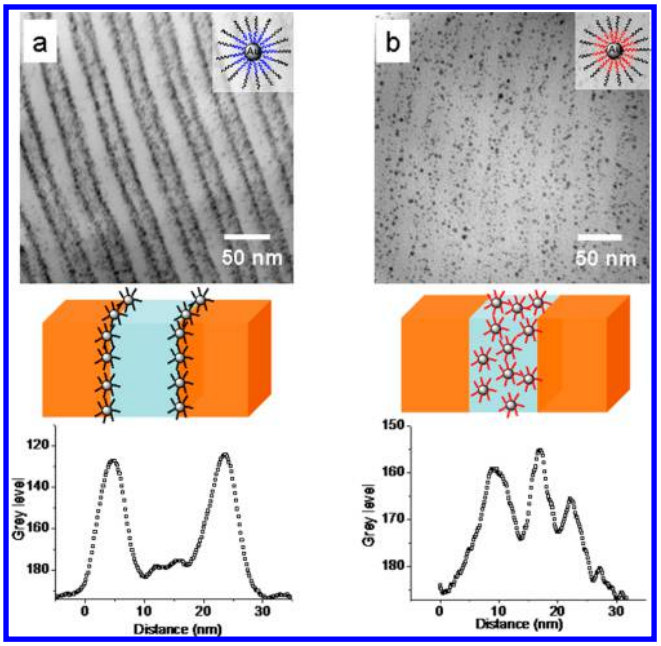

Figure 6. (a) TEM image together with the image analysis of the composites consisting of PS-*b*-P2VP block copolymer (199 kg/mol, $f_{p2vp} \sim 0.48$) and 20 wt % of GNPs (PS_{23}-*b*-$PNBA_9$S-Au). (b) The GNPs were exposed to UV (365 nm) light before mixing with the PS-*b*-P2VP block copolymer.

segregate at PS/P2VP interfaces as evidenced by the statistical analysis of the TEM image, whereas the GNPs after UV irradiation were sequestered into P2VP domains as indicated by Figure 6b together with the TEM image analysis. The random distribution of GNPs in P2VP is mainly determined by an enthalpy-driven self-assembly process as a result of the strong H-bonding interactions between PAA on the gold surface and the P2VP block of the PS-*b*-P2VP matrix (see Scheme 2).

Using the same PS-*b*-P2VP BCP (199 kg/mol, $f_{p2vp} \sim 0.48$), similar UV effects were observed on the self-assembly behaviors of the composites containing 15 wt % of GNPs (PS_{23}-*b*-$PNBA_{15}$S-Au) with more NBA units in the inner layer. The GNPs prior to UV irradiation are mainly segregated at the PS/P2VP interface (see Figure S3, Supporting Information), while GNPs after UV irradiation are randomly distributed in P2VP domains as illustrated by Figure 7a. The TEM of iodine-stained sample further confirmed the location of GNPs in darker regions (Figure S4, Supporting Information). Because of the formation of multiple H-bonds between PAA on GNPs and

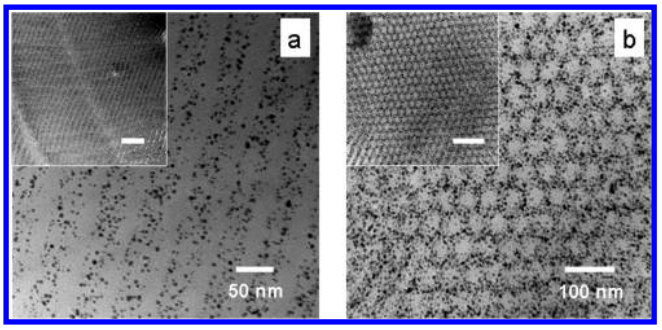

Figure 7. TEM images of the lamellae-forming PS-*b*-P2VP block copolymer (199 kg/mol, $f_{P2VP} \sim 0.48$) with GNPs (PS_{40}-*b*-$PNBA_{15}$S-Au) of different loadings: (a) 15 wt % (11 vol %); (b) 30 wt % (24 vol %). The GNPs were exposed to UV (365 nm) light before mixing with the PS-*b*-P2VP block copolymer. Scale bars in the insets are 200 nm.

P2VP of the BCP matrix, we have achieved a higher loading (30 wt %) of the UV-treated GNPs into the P2VP domains of the PS-*b*-P2VP BCP. Here, the volume percentage ($ø_{GNP}$) of GNPs (core + ligand) was estimated using the TGA data (Figure S2, Supporting Information) and the densities of the components (polymer ≈ 1.05 g/cm^3; gold ≈ 19.3 g/cm^3). The $ø_{GNP}$ values for samples in Figure 7 are about (a) 11 vol % and (b) 24 vol %, and the total volume percentages of P2VP and GNPs ($ø_{P2PV+GNP}$) are (a) 54 vol % and (b) 61 vol %. Interestingly, the increase of $ø_{GNP}$ from 11% to 24% results in the formation of inverse cylindrical packing of GNPs without macrophase separation from the BCP domains (see Figure 7b). The morphology transition from lamellar to inverse cylindrical P2VP is consistent with the previous report that a similar morphology transition was observed at high GNP loadings.[39] However, the ordered cylindrical morphology here is different from the disordered ones in the previous work.[39] The significant differences in nanoparticle structure and/or H-bond type might be the reason for the improved cylindrical structure.

■ CONCLUSIONS

We reported the facile synthesis of micelle-like GNPs capped with photoresponsive poly(styrene)-*b*-poly(*o*-nitrobenzene acrylate) (PS-*b*-PNBA) BCP ligands. PS is the outer layer of the corona, while PNBA is the inner layer and can be deprotected into a highly hydrophilic block containing poly(acrylic acid) (PAA) by simple exposure to UV light of 365 nm. Through this design, the surface properties of GNPs can be readily tuned through UV light in radiation. The self-assembly behaviors of these nanoparticles have been systematically investigated using a lamellae-forming PS-*b*-P2VP block copolymer as the matrix. GNPs before UV irradiation segregate along PS/P2VP interfaces predominantly determined by the neutral interactions between PS-*b*-PNBA ligand and P2VP of the PS-*b*-P2VP matrix. In contrast, UV-treated GNPs are randomly distributed in P2VP domains as a result of H-bonding interactions between PAA on the gold surface and P2VP of the PS-*b*-P2VP. Benefiting from the multiple H-bonds, GNPs can be selectively incorporated into P2VP domains at high loadings up to 30 wt % (24 vol %), which induced a morphology transition of P2VP from a lamellar to an ordered inverse cylindrical structure. This work demonstrates the ways of imparting photoresponsive characters to nanoparticles of various functional cores (magnetic, electric, or photonic) and to composite materials with well-ordered nanostructures.

dx.doi.org/10.1021/jp508212f | *J. Phys. Chem. B* 2014, 118, 12788−12795

■ ASSOCIATED CONTENT

Supporting Information

TEM images and corresponding core size distributions of GNPs; TGA of gold nanoparticles; TEM images of the nanocomposites. This material is available free of charge via the Internet at http://pubs.acs.org.

■ AUTHOR INFORMATION

Corresponding Author

*Tel: 413-545-2569. Fax: 413-545-0082. E-mail: watkins@polysci.umass.edu.

Notes

The authors declare no competing financial interest.

■ ACKNOWLEDGMENTS

This work was supported by the NSF Center for Hierarchical Manufacturing at the University of Massachusetts (CMMI-1025020).

■ REFERENCES

(1) Bockstaller, M. R.; Thomas, E. L. Optical Properties of Polymer-Based Photonic Nanocomposite Materials. *J. Phys. Chem. B* **2003**, *107*, 10017−10024.

(2) Cheng, J. Y.; Ross, C. A.; Chan, V. Z. H.; Thomas, E. L.; Lammertink, R. G. H.; Vancso, G. J. Formation of a Cobalt Magnetic Dot Array via Block Copolymer Lithography. *Adv. Mater.* **2001**, *13*, 1174−1178.

(3) Jaramillo, T. F.; Baeck, S. H.; Cuenya, B. R.; McFarland, E. W. Catalytic Activity of Supported Au Nanoparticles Deposited from Block Copolymer Micelles. *J. Am. Chem. Soc.* **2003**, *125*, 7148−7149.

(4) Mui, S. C.; Trapa, P. E.; Huang, B.; Soo, P. P.; Lozow, M. I.; Wang, T. C.; Cohen, R. E.; Mansour, A. N.; Mukerjee, S.; Mayes, A. M.; et al. Block Copolymer-templated Nanocomposite Electrodes for Rechargeable Lithium Batteries. *J. Electrochem. Soc.* **2002**, *149*, A1610−A1615.

(5) Warren, S. C.; Messina, L. C.; Slaughter, L. S.; Kamperman, M.; Zhou, Q.; Gruner, S. M.; DiSalvo, F. J.; Wiesner, U. Ordered Mesoporous Materials from Metal Nanoparticle-block Copolymer Self-assembly. *Science* **2008**, *320*, 1748−1752.

(6) Xiang, J.; Lu, W.; Hu, Y.; Wu, Y.; Yan, H.; Lieber, C. M. Ge/Si Nanowire Heterostructures as High-performance Field-effect Transistors. *Nature* **2006**, *441*, 489−493.

(7) Briseno, A. L.; Yang, P. Optoelectronics: Combining Chemical Worlds. *Nat. Mater.* **2009**, *8*, 7−8.

(8) Kao, J.; Thorkelsson, K.; Bai, P.; Rancatore, B. J.; Xu, T. Toward Functional Nanocomposites: Taking the Best of Nanoparticles, Polymers, and Small Molecules. *Chem. Soc. Rev.* **2013**, *42*, 2654−2678.

(9) Bockstaller, M. R.; Lapetnikov, Y.; Margel, S.; Thomas, E. L. Size-selective Organization of Enthalpic Compatibilized Nanocrystals in Ternary Block Copolymer/Particle Mixtures. *J. Am. Chem. Soc.* **2003**, *125*, 5276−5277.

(10) Chiu, J. J.; Kim, B. J.; Kramer, E. J.; Pine, D. J. Control of Nanoparticle Location in Block Copolymers. *J. Am. Chem. Soc.* **2005**, *127*, 5036−5037.

(11) Lin, Y.; Boker, A.; He, J. B.; Sill, K.; Xiang, H. Q.; Abetz, C.; Li, X. F.; Wang, J.; Emrick, T.; Long, S.; et al. Self-directed Self-assembly of Nanoparticle/ Copolymer Mixtures. *Nature* **2005**, *434*, 55−59.

(12) Balazs, A. C.; Emrick, T.; Russell, T. P. Nanoparticle Polymer Composites: Where Two Small Worlds Meet. *Science* **2006**, *314*, 1107−1110.

(13) Lee, J. Y.; Thompson, R. B.; Jasnow, D.; Balazs, A. C. Entropically Driven Formation of Hierarchically Ordered Nanocomposites. *Phys. Rev. Lett.* **2002**, *89*, 155503.

(14) Lee, J. Y.; Shou, Z. Y.; Balazs, A. C. Predicting the Morphologies of Confined Copolymer/Nanoparticle Mixtures. *Macromolecules* **2003**, *36*, 7730−7739.

(15) Kim, B. J.; Chiu, J. J.; Yi, G. R.; Pine, D. J.; Kramer, E. J. Nanoparticle-Induced Phase Transitions in Diblock-Copolymer Films. *Adv. Mater.* **2005**, *17*, 2618.

(16) Kim, B. J.; Bang, J.; Hawker, C. J.; Kramer, E. J. Effect of Areal Chain Density on the Location of Polymer-Modified Gold Nanoparticles in a Block Copolymer Template. *Macromolecules* **2006**, *39*, 4108−4114.

(17) Kim, B. J.; Bang, J.; Hawker, C. J.; Chiu, J. J.; Pine, D. J.; Jang, S. G.; Yang, S. M.; Kramer, E. J. Creating Surfactant Nanoparticles for Block Copolymer Composites through Surface Chemistry. *Langmuir* **2007**, *23*, 12693−12703.

(18) Park, S. C.; Kim, B. J.; Hawker, C. J.; Kramer, E. J.; Bang, J.; Ha, J. S. Controlled Ordering of Block Copolymer Thin Films by the Addition of Hydrophilic Nanoparticles. *Macromolecules* **2007**, *40*, 8119−8124.

(19) Chiu, J. J.; Kim, B. J.; Yi, G. R.; Bang, J.; Kramer, E. J.; Pine, D. J. Distribution of Nanoparticles in Lamellar Domains of Block Copolymers. *Macromolecules* **2007**, *40*, 3361−3365.

(20) Breiner, T.; Kreger, K.; Hagen, R.; Hackel, M.; Kador, L.; Muller, A. H. E.; Kramer, E. J.; Schmidt, H. W. Blends of Poly(methacrylate) Block Copolymers with Photoaddressable Segments. *Macromolecules* **2007**, *40*, 2100−2108.

(21) Kim, B. J.; Fredrickson, G. H.; Kramer, E. J. Effect of Polymer Ligand Molecular Weight on Polymer-Coated Nanoparticle Location in Block Copolymers. *Macromolecules* **2008**, *41*, 436−447.

(22) Tang, C. B.; Lennon, E. M.; Fredrickson, G. H.; Kramer, E. J.; Hawker, C. J. Evolution of Block Copolymer Lithography to Highly Ordered Square Arrays. *Science* **2008**, *322*, 429−432.

(23) Noro, A.; Matsushita, Y.; Lodge, T. P. Thermoreversible Supramacromolecular Ion Gels via Hydrogen Bonding. *Macromolecules* **2008**, *41*, 5839−5844.

(24) Noro, A.; Matsushita, Y.; Lodge, T. P Gelation Mechanism of Thermoreversible Supramacromolecular Ion Gels via Hydrogen Bonding. *Macromolecules* **2009**, *42*, 5802−5810.

(25) Dobrosielska, K.; Takano, A.; Matsushita, Y. Creation of Hierarchical Nanophase-Separated Structures via Supramacromolecular Self-Assembly from Two Asymmetric Block Copolymers with Short Interacting Sequences Giving Hydrogen Bonding Interaction. *Macromolecules* **2010**, *43*, 1101−1107.

(26) Dobrosielska, K.; Wakao, S.; Takano, A.; Matsushita, Y. Nanophase-Separated Structures of AB Block Copolymer/C Homopolymer Blends with Complementary Hydrogen-Bonding Interactions. *Macromolecules* **2008**, *41*, 7695−7698.

(27) Dobrosielska, K.; Wakao, S.; Suzuki, J.; Noda, K.; Takano, A.; Matsushita, Y. Effect of Homopolymer Molecular Weight on Nanophase-Separated Structures of AB Block Copolymer/C Homopolymer Blends with Hydrogen-Bonding Interactions. *Macromolecules* **2009**, *42*, 7098−7102.

(28) Chen, S. C.; Kuo, S. W.; Jeng, U. S.; Su, C. J.; Chang, F. C. On Modulating the Phase Behavior of Block Copolymer/Homopolymer Blends via Hydrogen Bonding. *Macromolecules* **2010**, *43*, 1083−1092.

(29) Li, Q. F.; He, J. B.; Glogowski, E.; Li, X. F.; Wang, J.; Emrick, T.; Russell, T. P. Responsive Assemblies: Gold Nanoparticles with Mixed Ligands in Microphase Separated Block Copolymers. *Adv. Mater.* **2008**, *20*, 1462.

(30) Zhao, Y.; Thorkelsson, K.; Mastroianni, A. J.; Schilling, T.; Luther, J. M.; Rancatore, B. J.; Matsunaga, K.; Jinnai, H.; Wu, Y.; Poulsen, D.; et al. Small-Molecule-Directed Nanoparticle Assembly Towards Stimuli-Responsive Nanocomposites. *Nat. Mater.* **2009**, *8*, 979−985.

(31) Lin, Y.; Daga, V. K.; Anderson, E. R.; Gido, S. P.; Watkins, J. J. Nanoparticle-Driven Assembly of Block Copolymers: A Simple Route to Ordered Hybrid Materials. *J. Am. Chem. Soc.* **2011**, *133*, 6513−6516.

(32) Wei, Q. S.; Lin, Y.; Anderson, E. R.; Briseno, A. L.; Gido, S. P.; Watkins, J. J. Additive-Driven Assembly of Block Copolymer−Nanoparticle Hybrid Materials for Solution Processable Floating Gate Memory. *ACS Nano* **2012**, *6*, 1188−1194.

(33) Yao, L.; Lin, Y.; Watkins, J. J. Ultrahigh Loading of Nanoparticles into Ordered Block Copolymer Composites. *Macromolecules* **2014**, *47*, 1844−1849.
(34) Daga, V. K.; Anderson, E. R.; Gido, S. P.; Watkins, J. J. Hydrogen Bond Assisted Assembly of Well-Ordered Polyhedral Oligomeric Silsesquioxane−Block Copolymer Composites. *Macromolecules* **2011**, *44*, 6793−6799.
(35) Daga, V. K.; Watkins, J. J. Hydrogen-Bond-Mediated Phase Behavior of Complexes of Small Molecule Additives with Poly(ethylene oxide-b-propylene oxide-b-ethylene oxide) Triblock Copolymer Surfactants. *Macromolecules* **2010**, *43*, 9990−9997.
(36) Tirumala, V. R.; Daga, V.; Bosse, A. W.; Romang, A.; Ilavsky, J.; Lin, E. K.; Watkins, J. J. Well-Ordered Polymer Melts with 5 nm Lamellar Domains from Blends of a Disordered Block Copolymer and A Selectively Associating Homopolymer of Low or High Molar Mass. *Macromolecules* **2008**, *41*, 7978−7985.
(37) Tirumala, V. R.; Romang, A.; Agarwal, S.; Lin, E. K.; Watkins, J. J. Well Ordered Polymer Melts from Blends of Disordered Triblock Copolymer Surfactants and Functional Homopolymers. *Adv. Mater.* **2008**, *20*, 1603−1608.
(38) Jang, S. G.; Kramer, E. J.; Hawker, C. J. Controlled Supramolecular Assembly of Micelle-like Gold Nanoparticles in PS-b-P2VP Diblock Copolymers via Hydrogen Bonding. *J. Am. Chem. Soc.* **2011**, *133*, 16986−16996.
(39) Jang, S. G.; Khan, A.; Hawker, C. J.; Kramer, E. J. Morphology Evolution of PS-b-P2VP Diblock Copolymers via Supramolecular Assembly of Hydroxylated Gold Nanoparticles. *Macromolecules* **2012**, *45*, 1553−1561.
(40) Yee, C. K.; Jordan, R.; Ulman, A.; White, H.; King, A.; Rafailovich, M.; Sokolov, J. Novel One-Phase Synthesis of Thiol-Functionalized Gold, Palladium, and Iridium Nanoparticles Using Superhydride. *Langmuir* **1999**, *15*, 3486−3491.
(41) Yao, L.; Watkins, J. J. Photoinduced Disorder in Strongly Segregated Block Copolymer Composite Films for Hierarchical Pattern Formation. *ACS Nano* **2013**, *7*, 1513−1523.
(42) Daga, V. K.; Schwartz, E. L.; Chandler, C. M.; Lee, J. K.; Lin, Y.; Ober, C. K.; Watkins, J. J. Photoinduced Ordering of Block Copolymers. *Nano Lett.* **2011**, *11*, 1153−1160.
(43) Zhao, H.; Sterner, E. S.; Coughlin, E. B.; Theato, P. o-Nitrobenzyl Alcohol Derivatives: Opportunities in Polymer and Materials Science. *Macromolecules* **2012**, *45*, 1723−1736.
(44) Il'ichev, Y. V.; Schworer, M. A.; Wirz, J. Photochemical Reaction Mechanisms of 2-Nitrobenzyl Compounds: Methyl Ethers and Caged ATP. *J. Am. Chem. Soc.* **2004**, *126*, 4581−4595.
(45) Pelliccioli, A. P.; Wirz, J. Photoremovable Protecting Groups: Reaction Mechanisms and Applications. *Photochem. Photobiol. Sci.* **2002**, *1*, 441−458.
(46) Schumers, J.; Fustin, C.; Can, A.; Hoogenboom, R.; Schubert, U. S.; Gohy, J. F. Are o-Nitrobenzyl (meth)Acrylate Monomers Polymerizable by Controlled-Radical Polymerization? *J. Polym. Sci., Part A: Polym. Chem.* **2009**, *47*, 6504−6513.
(47) Kim, B. J.; Fredrickson, G. H.; Hawker, C. J.; Kramer, E. J. Nanoparticle Surfactants as A Route to Bicontinuous Block Copolymer Morphologies. *Langmuir* **2007**, *23*, 7804−7809.
(48) Kim, B. J.; Fredrickson, G. H.; Bang, J.; Hawker, C. J.; Kramer, E. J. Tailoring Core−Shell Polymer-Coated Nanoparticles as Block Copolymer Surfactants. *Macromolecules* **2009**, *42*, 6193−6201.
(49) Thompson, R. B.; Ginzburg, V. V.; Matsen, M. W.; Balazs, A. C. Predicting the Mesophases of Copolymer-Nanoparticle Composites. *Science* **2001**, *292*, 2469−2472.
(50) Huh, J.; Ginzburg, V. V.; Balazs, A. C. Thermodynamic Behavior of Particle/Diblock Copolymer Mixtures: Simulation and Theory. *Macromolecules* **2000**, *33*, 8085−8096.